Non-Singular Transformation for Inverting Gravity Anomalies Using Satellite Altimetry Data

ZONG JINGWEN[1], **(Member, IEEE), BIAN SHAOFENG**[1], **LI HOUPU**[1], **JI BING**[1], **AND OUYANG YONGZHONG**[2]

[1]Department of Navigation, College of Electrical Engineering, Naval University of Engineering, Wuhan 430033, China
[2]Key Laboratory of Marine Environmental Survey Technology and Application, Ministry of Natural Resources, Guangzhou 510260, China

Corresponding author: Li Houpu (lihoupu1985@126.com)

ABSTRACT Traditional measurement methods, like shipborne and aerial gravity measurements, cannot cover the entire sea area. Satellite altimetry provides large-scale and high-precision observational data, which can be inverted to give high-precision and high-resolution data on marine gravity anomalies. In this paper, to improve the precision of computing the innermost zone effects in gravitational altimetry data, the deflections of the vertical are expressed in the form of double cubic polynomials by treating the innermost zone as a rectangle, based on the inverse Vening Meinesz formula. Furthermore, formulas for computing gravity anomalies in the innermost zone are derived using a non-singular transformation. The numerical experiments show that the relative error of the algorithm in this paper, which uses a non-singular transformation, is less than 1.5%. Moreover, the practical computational results based on deflections of the vertical for data with a resolution of 2' × 2' from the South China Sea and its vicinity also demonstrate that gravity anomalies in the innermost zone have a non-negligible contribution when using a non-singular transformation.

INDEX TERMS Satellite altimetry, non-singular transformation, gravity anomaly, inverse Vening Meinesz formula, deflection of the vertical, innermost zone effects.

I. INTRODUCTION

Marine gravity anomalies reflect the internal structure of the ocean, including the topography of the marine floor and the geoid. They are widely used to construct the geoid, in dynamic marine environmental research, and in offshore oil and gas exploration. At present, marine gravity field data are obtained from satellite altimetry inversion and from shipborne and aerial gravity measurements. With the development of artificial Earth satellite technology, satellite altimetry technology has promoted the interdisciplinary development of geodesy, geophysics, and oceanography. In the 1970s, the emergence of satellite altimetry technology and the smooth implementation of multiple satellite altimetry missions greatly facilitated the collection of high-precision

The associate editor coordinating the review of this manuscript and approving it for publication was Gerardo Di Martino.

and high-resolution sea-level data from oceans around the globe [1].

Altogether, 18 major altimetry satellites have been launched by various countries over the past 40 years, including Geosat launched by the United States Navy, TOPEX/Poseidon (T/P), Jason-1 [2], [3], Jason-2 [4]–[6], and Jason-3 launched by the National Aeronautics and Space Administration and French Centre National d'Etudes Spatiales, the European Remote-Sensing Satellites (ERS series) launched by the European Space Agency, and Haiyang-2A (HY-2A) launched by China [7], [8]. There are early altimetry satellites (Skylab, GEOS-3, and Seasat), military altimetry satellites (Geosat and Geosat Follow-On), marine integrated environmental monitoring satellites (ERS-1, ERS-2, and Envisat), marine terrain observation satellites (T/P, Jason-1, Jason-2, and Jason-3), and polar observation satellites (ICESat, Sentinel-3A, and CryoSat-2).

The main aims of the Geosat series were to measure the ocean geoid accurately and to provide wind speed and ocean observation data. The data are widely used in studies of the geoid, ocean gravity anomalies, and ocean numerical models. They have a high accuracy of 5–10 cm.

The main goals of the T/P series were to study global sea level changes and ocean circulation. The data are used to study ocean phenomena and global climate change. They have a high accuracy of 2–3 cm.

The ERS series mainly observed the polar ice caps, ocean circulation, and sea surface height. They made high-precision measurements of the sea surface topography, and ocean and land surface temperatures. Finally, HY-2A was mainly used to record the dynamic marine environment.

Satellite altimetry data cover all the oceans from 85°S to 85°N on a 2' × 2' grid across the globe and have an accuracy of 1–2 cm [9]. Moreover, the accuracy of the inversion of a gravity anomaly from satellite altimetry data has reached 4×10^{-6} to 10×10^{-6} m/s^2.

Researchers from several institutions have performed a considerable amount of research on satellite altimetry. Li *et al.* [10] from Wuhan University used the Laplace equation to invert gravity anomalies of the global sea. The accuracy of the 1' × 1' gravity field model of the global sea and ship survey data from the National Geophysical Data Center was 4×10^{-6} to 8×10^{-6} m/s^2. Huang *et al.* [11], [12] from the Naval Research Institute of the People's Liberation Army developed and studied three methods (analytical and numerical inversion of the Stokes formula, and the inverse Vening Meinesz formula) for identifying gravity anomalies from altimeter data. Hsu *et al.* [13] from the Chinese Academy of Sciences used the inverse Stokes formula to invert gravity anomalies in the China Sea, achieving an accuracy of $3.5 \times 10^{-6} 3.5 \times 10^{-6}$ m/s^2. In addition, Sandwell *et al.* [14], [15] from the Scripps Institution of Oceanography, Andersen *et al.* [16], [17] from the Technical University of Denmark, and Hwang *et al.* [18] from National Chiao Tung University used Geosat and ERS-1 altimetry data to identify global ocean gravity anomalies. These researchers have made many contributions in the fusion and fine processing of satellite altimetry data.

Usually, the input to the inverse Vening Meinesz formula is deflections of the vertical, which are obtained from the first-order difference of altimetry observations. This approach eliminates the radial orbit errors due to changes in the geographical position and long waves on the sea surface, as well as other similar systemic errors. The deflections of the vertical have rich high-frequency components of the gravity field, which are useful in calculating a high-resolution ocean gravity field. With the advent of satellite altimetry, deflections of the vertical have become available for the oceans and the inverse Vening Meinesz formula can be useful in computing marine gravity from satellite altimetry. Therefore, the inverse Vening Meinesz formula is widely used for altimetry gravity inversion. Moreover, Gopalapillai [19] transformed satellite altimetry data into gravity anomalies

using the Stokes formula. Sandwell and Smith [20] proposed a method for inverting gravity anomalies based on deflections of the vertical and systematically provided expressions for the relations among the deflections of the vertical, disturbing gravity, and a gravity anomaly.

However, in the actual evaluation of a gravity anomaly at the target point and nearby areas, the integration area contains the target point. In this case, the inverse Stokes formula and the inverse Vening Meinesz formula use singular integration. The integration area is called the innermost zone [21], [22]. In the literature, the calculation point of the integral kernel function is usually set to zero. This, however, ignores the influence of the innermost zone on the gravity anomaly. Given that a fast Fourier transformation requires the input to be the geoid height for the regular grid, the smallest area in the innermost zone is one grid element. Considering the resolution of satellite altimetry data, the innermost zone of the inverse Vening Meinesz formula is likely to be an area ranging from several thousand to tens of thousands of square kilometers. Whether the influence of this area on the gravity anomaly can be neglected still needs further study.

Bian [23] proposed a set of non-singular transformations that systematically solved the innermost zone calculation problems for the height anomaly, deflections of the vertical, terrain correction, and gravity anomaly in physical geodesy. Hwang *et al.* [24], [25] regarded the innermost zone as a circle and derived formulas for gravity anomalies in the innermost zone. However, the gravity anomalies are in rectangular grids (such as 2' × 2'). If approximation series are used, significant approximation errors may be introduced. Chang *et al.* [9] dealt with the innermost zone as a square domain and derived a formula for the innermost zone effects. They noted that these effects for a gravity anomaly depend on the gradients of the deflection components [26] and the size of the singular area. The actual data are usually distributed in a grid, and then the innermost zone can be approximated as a rectangle due to meridian convergence. Therefore, processing methods that treat the central area as a circle or a square do not match the actual distribution of the data. Whether such an error can be ignored in high-precision gravity inversion requires further study. Sunkel [27] and Wang [28] expressed gravity anomalies block by block using an interpolation polynomial and derived analytic values for the integrals. However, the integrals of these rational functions are highly complex, especially when the related interpolation polynomials have many terms. Only the analytic values of the corresponding linear approximation can be obtained.

To assess the computational accuracy of the inversion of satellite altimetry data for a gravity anomaly, we compare the results from using and not using the non-singular transformation. In Section II, we derive a formula for a gravity anomaly by treating the innermost zone as a rectangle and use the non-singular integration transformations proposed by [29]. Then, in Section III, the theoretical model and the actual data are used to analyze the contribution of the innermost zone. Finally, numerical experiments on the influence
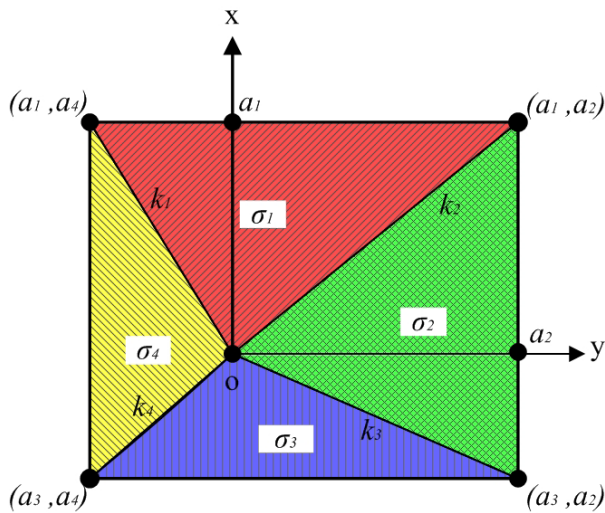
FIGURE 1. Local rectangular coordinates of the integral zone.

of the innermost zone effect on gravity anomalies are described.

II. THEORETICAL MODEL

A. NON-SINGULAR TRANSFORMATION METHOD

There is a class of singular integrals related to the reciprocal distance in the evaluation of the Earth's gravity field. For example, when the height anomalies, deflections of the vertical, and gravity gradients use planar approximations, they can be expressed as the convolution.

$$
\begin{cases}
\zeta = \dfrac{1}{2\pi\gamma} \iint \dfrac{\Delta g(x,y)}{r} \mathrm{d}x\mathrm{d}y, \\
\xi = -\dfrac{1}{2\pi\gamma} \iint \dfrac{\Delta g(x,y)x}{r^3} \mathrm{d}x\mathrm{d}y, \\
\eta = -\dfrac{1}{2\pi\gamma} \iint \dfrac{\Delta g(x,y)y}{r^3} \mathrm{d}x\mathrm{d}y, \\
\dfrac{\partial \Delta g}{\partial h} = \dfrac{1}{2\pi} \iint \dfrac{\Delta g(x,y) - \Delta g_P}{r^3} \mathrm{d}x\mathrm{d}y,
\end{cases} \tag{1}
$$

where x is the longitudinal coordinate, y is the horizontal coordinate, ζ is the height anomaly, ξ and η are the deflections of the vertical, $\partial \Delta g/\partial h$ is the gravity gradient, and Δg is the gravity anomaly. When $r \to 0$, the above integrals are all singular. A numerical evaluation of the gravity field on or near the singular points is usually difficult, and the accuracy of the gravity field is limited. This paper introduces a set of non-singular transformation that make the singular integrals non-singular so that it is possible to directly implement numerical integration in the innermost area.

The singular integrals depend on the selection of the variable. The general treatment in mathematical analysis is to replace the variable to transform the singular integrals into non-singular integrals.

Fig. 1 shows the local rectangular coordinates of the integral zone. O is the origin of the rectangular coordinate system, the x is the x-axis, the y is the y-axis. The

integral area is a rectangle. It is divided into four areas (σ_1, σ_2, σ_3, and σ_4) by connecting the point O to the four vertices. k_1, k_2, k_3, and k_4 are the slopes of each line connecting point O to a vertex. The perpendicular distances from point O to each side are a_1, a_2, a_3, and a_4. The scopes of the areas σ_1, σ_2, σ_3, and σ_4 can be expressed as follows: $\sigma_1 \in [(x,y)| 0 < x < a_1, k_1 x < y < k_2 x]$, $\sigma_2 \in [(x,y)| y/k_3 < x < y/k_2, 0 < y < a_2]$, $\sigma_3 \in [(x,y)| a_3 < x < 0, k_4 x < y < k_3 x]$, and $\sigma_4 \in [(x,y)| y/k_1 < x < y/k_4, a_4 < y < 0]$. For example, the integral is $A = \iint 1/r\, \mathrm{d}\sigma = \iint 1/r\, \mathrm{d}x\mathrm{d}y$. When $r \to 0$, this integral is singular.

First, the non-singular transformation is introduced using σ_1 as an example:

$$
\begin{cases}
x = x, \\
y = x \cdot z.
\end{cases} \tag{2}
$$

Then, the determinant of the corresponding Jacobi matrix can be obtained:

$$
\det(\mathbf{J}) = \left| \frac{\partial(x,y)}{\partial(x,z)} \right| = \begin{vmatrix} \dfrac{\partial x}{\partial x} & \dfrac{\partial x}{\partial z} \\ \dfrac{\partial y}{\partial x} & \dfrac{\partial y}{\partial z} \end{vmatrix} = \begin{vmatrix} 1 & 0 \\ z & x \end{vmatrix} = x. \tag{3}
$$

Finally, the singular integral can be transformed into a non-singular integral through the above steps. σ_1 is replaced by $\sigma_1' \in [(x,z)| 0 < x < a_1, k_1 < z < k_2]$:

$$
A = \iint \frac{\mathrm{d}\sigma}{r} = \iint \frac{\mathrm{d}x\mathrm{d}y}{\sqrt{x^2 + y^2}} = \iint \frac{|\mathbf{J}|\,\mathrm{d}x\mathrm{d}z}{\sqrt{x^2 + x^2 z^2}}
$$
$$
= \iint \frac{\mathrm{d}x\mathrm{d}z}{\sqrt{1 + z^2}}, \tag{4}
$$

where $\mathrm{d}\sigma = \mathrm{d}x \cdot \mathrm{d}y$, $r = \sqrt{x^2 + y^2}$.

B. PLANE APPROXIMATION OF THE INVERSE VENING MEINESZ FORMULA

From Hwang [24], the inverse Vening Meinesz formula is:

$$
\Delta g_P = \frac{\gamma_0}{4\pi} \iint_\sigma H'(\psi_{PQ}) \left(\xi_Q \cos\alpha_{QP} + \eta_Q \sin\alpha_{QP} \right) \mathrm{d}\sigma \tag{5}
$$

where Δg_P is a gravity anomaly at the computation point P, $\gamma_0 = 979.8 \times 10^{-3}$ m/s^2 is the average value of Earth's gravity, Q is a random point, α_{QP} is the azimuth from point Q to point P, ψ_{PQ} is the spherical angular distance from point P to point Q, ξ_Q is the component of the deflections of the vertical in the north–south direction at point Q, and η_Q is the component of the deflections of the vertical in the east–west direction at the point Q. Here, $H'(\psi_{PQ})$ is the integral kernel function [30]:

$$
H'(\psi_{PQ}) = -\frac{\cos(\psi_{PQ}/2)}{2\sin^2(\psi_{PQ}/2)}
$$
$$
+ \frac{\cos(\psi_{PQ}/2)\left(3 + 2\sin(\psi_{PQ}/2)\right)}{2\sin(\psi_{PQ}/2)\left(1 + \sin(\psi_{PQ}/2)\right)}. \tag{6}
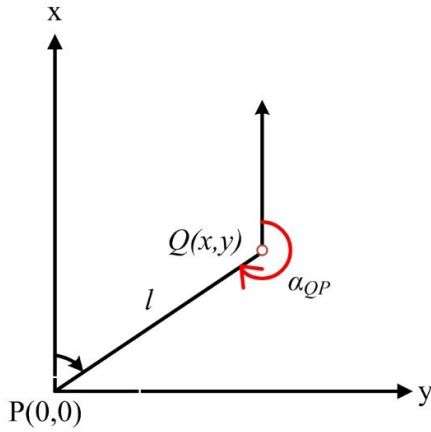$$

FIGURE 2. The local rectangular coordinate frame.

To evaluate the gravity anomaly in the innermost zone, we construct the Cartesian coordinate frame at the local tangent plane where the point P is the origin.

In the local rectangular coordinate frame shown in Fig. 2, the x-axis points to the north, the y-axis points to the east, the xy-plane is tangent to the surface of the Earth at the point P, $Q(x, y)$ is the dynamic integration points in the innermost zone, and l is the distance between points P and Q. Moreover, it can be seen from Fig. 2 that:

$$\begin{cases} \cos \alpha_{QP} = -\dfrac{x}{l}, \\ \sin \alpha_{QP} = -\dfrac{y}{l}, \end{cases} \tag{7}$$

where $l = \sqrt{x^2 + y^2}$. When the integration area is small, the spherical distance ψ_{PQ} can be approximated as $\psi_{PQ} \approx l/R$. Where R is mean radius of the earth. As a result, the integral kernel function in (5) can be approximated as:

$$H'(\psi_{PQ})$$
$$= -\frac{\cos(\psi_{PQ}/2)}{2\sin^2(\psi_{PQ}/2)} + \frac{\cos(\psi_{PQ}/2)\left(3 + 2\sin(\psi_{PQ}/2)\right)}{2\sin(\psi_{PQ}/2)\left(1 + \sin(\psi_{PQ}/2)\right)}$$
$$\approx -\frac{\cos(\psi_{PQ}/2)}{2\sin^2(\psi_{PQ}/2)} + \frac{3\cos(\psi_{PQ}/2)}{2\sin(\psi_{PQ}/2)}$$
$$\approx \frac{1}{2(\psi_{PQ}/2)^2} = \frac{2}{\psi_{PQ}^2} = -\frac{2R^2}{l^2}. \tag{8}$$

Substituting, equations (7) and (8) into equation (5), and because $R^2 d\sigma = dxdy$, the gravity anomaly in the innermost zone can be simplified as:

$$\Delta g_P$$
$$= \frac{\gamma}{4\pi} \iint_\sigma \left(-\frac{2R^2}{l^2}\right) \cdot \left(\left(-\frac{x}{l}\right) \cdot \xi_Q + \left(-\frac{y}{l}\right) \cdot \eta_Q\right) \cdot \frac{1}{R^2} dxdy$$
$$= \frac{\gamma}{2\pi} \iint_\sigma \frac{\xi_Q \cdot x + \eta_Q \cdot y}{(x^2 + y^2)^{3/2}} dxdy. \tag{9}$$

When $l \rightarrow 0$, the above integrals become singular. To solve this problem, Hwang regarded the innermost zone

as a circular area and expanded ξ_Q and η_Q into Taylor series forms:

$$\begin{cases} \xi(x, y) = \xi_P + \xi_x x + \xi_y y + \dfrac{1}{2!}(\xi_{xx} x^2 \\ \qquad\qquad + 2\xi_{xy} xy + \xi_{yy} y^2) + \cdots \\ \eta(x, y) = \eta_P + \eta_x x + \eta_y y + \dfrac{1}{2!}(\eta_{xx} x^2 \\ \qquad\qquad + 2\eta_{xy} xy + \eta_{yy} y^2) + \cdots \end{cases} \tag{10}$$

Retaining only the linear terms in equation (10) and assuming that the innermost zone is circular, the gravity anomaly of the innermost zone can be written as:

$$\Delta g_1 = \frac{\gamma_0}{2} \cdot \sqrt{\frac{\Delta x \cdot \Delta y}{\pi}} \cdot (\xi_x + \eta_y) \tag{11}$$

where Δx is the grid spacing in the x direction and Δy is the grid spacing in the y direction.

Chang *et al.* [9] regarded the innermost zone as a square domain and expanded ξ_Q and η_Q into Taylor series forms (equations (10)). Then, the gravity anomaly of the innermost zone can be written as:

$$\Delta g_2 = \frac{2 \cdot \ln\left(1 + \sqrt{2}\right)}{\pi} \cdot s \cdot \gamma_0 \cdot (\xi_x + \eta_y), \tag{12}$$

where s is the half the length of the square domain.

C. THE ACCURATE FORMULA FOR SATELLITE ALTIMETRY IN THE INNERMOST ZONE

The deflections of the vertical can be expressed using bicubic interpolation by treating the innermost zone as a rectangle. In mathematics, bicubic interpolation is an extension of cubic interpolation for data points on a two-dimensional regular grid. The interpolated surface is smoother than the corresponding surfaces obtained by bilinear interpolation or nearest-neighbor interpolation. Bicubic interpolation can be accomplished using Lagrange polynomials, cubic splines, or cubic convolution. Next, we derive formulas for evaluating the gravity anomaly of this area using the non-singular transformation [31].

1) DEFLECTIONS OF THE VERTICAL EXPRESSED BY BICUBIC INTERPOLATION IN THE INNERMOST ZONE

As shown in Fig. 3, σ is the supposed integration area of the innermost zone: $\sigma \in [(x, y)| - 3a/2 < x < 3a/2, \ -3b/2 < y < 3b/2], (a > 0, b > 0)$. ξ_Q and η_Q can be expressed using bicubic interpolation as follows:

$$\xi(x, y) = \sum_{i=0}^{3} \left(\frac{x}{a}\right)^i \sum_{j=0}^{3} \alpha_{ij} \left(\frac{y}{b}\right)^j \tag{13}$$

$$\eta(x, y) = \sum_{i=0}^{3} \left(\frac{x}{a}\right)^i \sum_{j=0}^{3} \beta_{ij} \left(\frac{y}{b}\right)^j. \tag{14}$$
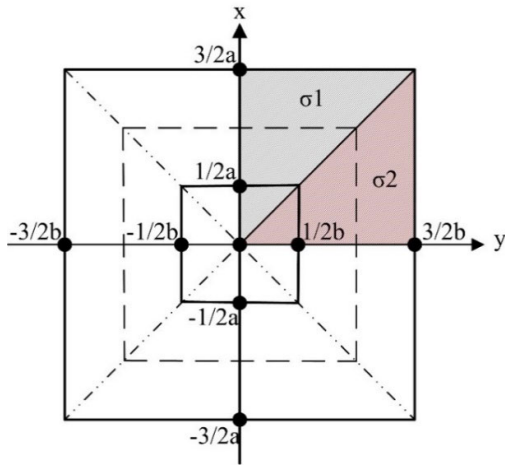
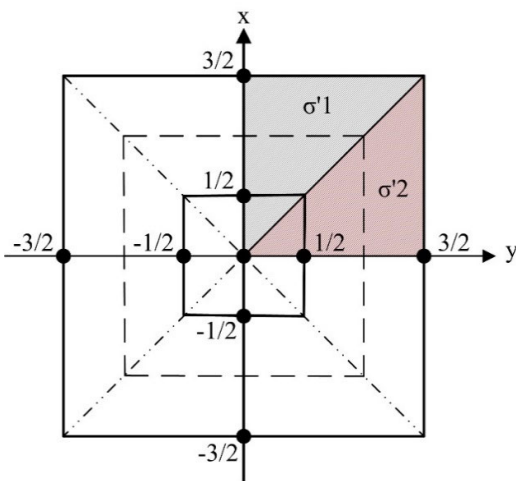**FIGURE 3.** Integral domains in the rectangular area.

FIGURE 4. Innermost zone after variable transformations.

To simplify the integration, two new coordinate variables are introduced:

$$\begin{cases} u = \dfrac{x}{a}, \\ v = \dfrac{y}{b}. \end{cases} \tag{15}$$

Hence, equations (13) and (14) become

$$\begin{cases} \xi(x, y) = \displaystyle\sum_{i=0}^{3} u^i \sum_{j=0}^{3} \alpha_{ij} v^j, \\ \eta(x, y) = \displaystyle\sum_{i=0}^{3} u^i \sum_{j=0}^{3} \beta_{ij} v^j. \end{cases} \tag{16}$$

The integration area of the innermost zone can be described by: $\sigma' \in [(u, v)| -3/2 < u < 3/2, -3/2 < v < 3/2]$.

In Fig. 4, $\xi_{ij} = \xi(i + 1/2, j + 1/2)$ and $\eta_{ij} = \eta(i + 1/2, j + 1/2)$ on grid nodes can be considered as the interpolation conditions in equation (16). Thus, equation (16) can be

simplified as:

$$A(\boldsymbol{\alpha})A^T = (\boldsymbol{\xi}), \tag{17}$$
$$A(\boldsymbol{\beta})A^T = (\boldsymbol{\eta}), \tag{18}$$

where

$$(\boldsymbol{\alpha}) = A^{-1}(\xi)(A^{-1})^T, \tag{19}$$
$$(\boldsymbol{\beta}) = A^{-1}(\eta)(A^{-1})^T. \tag{20}$$

Therefore, the undetermined coefficients $\boldsymbol{\alpha}$ and $\boldsymbol{\beta}$ are (21) and (22), as shown at the bottom of the next page.

2) FORMULAS TO EVALUATE A GRAVITY ANOMALY IN THE INNERMOST ZONE

Substituting equations (15) and (16) into equation (5), considering the integral nature of odd and even functions, and exploiting the symmetry of the integration area, then the gravity anomaly of the innermost zone is

$$\begin{aligned} \Delta g_P &= \frac{4\gamma a^2 b}{2\pi} \\ &\times \int_0^{3/2} \int_0^{3/2} \frac{(\alpha_{10} + \alpha_{12}v^2 + \alpha_{30}u^2 + \alpha_{32}u^2 v^2)u^2}{(a^2 u^2 + b^2 v^2)^{3/2}}\, du\, dv \\ &+ \frac{4\gamma a b^2}{2\pi} \int_0^{3/2} \\ &\times \int_0^{3/2} \frac{(\beta_{01} + \beta_{21}u^2 + \beta_{03}v^2 + \beta_{23}u^2 v^2)v^2}{(a^2 u^2 + b^2 v^2)^{3/2}}\, du\, dv, \quad (23) \end{aligned}$$

where $\sigma_1 \in [0 < u < 3/2, 0 < v < u]$ and $\sigma_2 \in [0 < u < v, 0 < v < 3/2]$. To simplify (23), we introduce

$$\begin{aligned} \Delta g_\xi &= \frac{4\gamma a^2 b}{2\pi} \\ &\times \int_0^{3/2} \int_0^{3/2} \frac{(\alpha_{10} + \alpha_{12}v^2 + \alpha_{30}u^2 + \alpha_{32}u^2 v^2)u^2}{(a^2 u^2 + b^2 v^2)^{3/2}}\, du\, dv, \end{aligned} \tag{24}$$

$$\begin{aligned} \Delta g_\eta &= \frac{4\gamma a^2 b}{2\pi} \\ &\times \int_0^{3/2} \int_0^{3/2} \frac{(\beta_{10} + \beta_{12}v^2 + \beta_{30}u^2 + \beta_{32}u^2 v^2)u^2}{(a^2 u^2 + b^2 v^2)^{3/2}}\, du\, dv \end{aligned} \tag{25}$$

with $\Delta g_P = \Delta g_\xi + \Delta g_\eta$. The integrals in equation (23) are singular. Thus, the non-singular transformation is introduced. The following non-singular integration transformation is introduced for the integrals in σ_1:

$$\begin{cases} u = u, \\ k = \dfrac{v}{u}. \end{cases} \tag{26}$$

Likewise, the following non-singular integration transformation is introduced for the integrals in σ_2:

$$\begin{cases} v = v, \\ \lambda = \dfrac{u}{v}. \end{cases} \tag{27}$$

Hence, $\sigma_1 \in [0 < u < 1, 0 < k < 1]$ and $\sigma_2 \in [0 < \lambda < 1, 0 < v < 1]$. Inserting equations (26) and (27) into equations (24) and (25), respectively, we arrive at

$$\begin{aligned} \Delta g_\xi = \frac{4\gamma a^2 b}{2\pi} \int_0^1 (\frac{3}{2}\alpha_{10} + \frac{9}{8}\alpha_{12}k^2 + \frac{9}{8}\alpha_{30} \\ + \frac{243}{160}\alpha_{32}k^2)\frac{\mathrm{d}k}{(a^2 + b^2k^2)^{3/2}} \\ + \frac{4\gamma a^2 b}{2\pi} \int_0^1 (\frac{3}{2}\alpha_{10} + \frac{9}{8}\alpha_{12} + \frac{9}{8}\alpha_{30}\lambda^2 \\ + \frac{243}{160}\alpha_{32}\lambda^2)\frac{\lambda^2 \mathrm{d}\lambda}{(b^2 + a^2\lambda^2)^{3/2}}, \end{aligned} \tag{28}$$

$$\begin{aligned} \Delta g_\eta = \frac{4ab^2}{2\pi\gamma} \int_0^1 (\frac{3}{2}\beta_{01} + \frac{9}{8}\beta_{21} + \frac{9}{8}\beta_{03}k^2 \\ + \frac{243}{160}\beta_{23}k^2)\frac{k^2 \mathrm{d}k}{(a^2 + b^2k^2)^{3/2}} \\ + \frac{4\gamma ab^2}{2\pi} \int_0^1 (\frac{3}{2}\beta_{01} + \frac{9}{8}\beta_{21}\lambda^2 + \frac{9}{8}\beta_{03} \\ + \frac{243}{160}\beta_{23}\lambda^2)\frac{\mathrm{d}\lambda}{(b^2 + a^2\lambda^2)^{3/2}}. \end{aligned} \tag{29}$$

Now we can see that the denominators are greater than zero in transformed equations (28) and (29), and the singularities have been eliminated. This basically changes the double integrals to single variable integrals, and the equation (23) can be evaluated [32], [33]: (30), as shown at the bottom of the next page, where $m = a/b$. The integration area of the innermost zone is $\sigma_1 \in [(u, v)| - 3/2 < u < 3/2, -3/2 < v < 3/2]$. The gravity anomaly in the 1×1 grid can be obtained in the same way as we obtained (30) in (31), as shown at the bottom of the next page.

$$\begin{pmatrix} \alpha_{00} & \alpha_{01} & \alpha_{02} & \alpha_{03} \\ \alpha_{10} & \alpha_{11} & \alpha_{12} & \alpha_{13} \\ \alpha_{20} & \alpha_{21} & \alpha_{22} & \alpha_{23} \\ \alpha_{30} & \alpha_{31} & \alpha_{32} & \alpha_{33} \end{pmatrix} = \begin{pmatrix} -\dfrac{1}{16} & \dfrac{9}{16} & \dfrac{9}{16} & -\dfrac{1}{16} \\ \dfrac{1}{24} & -\dfrac{9}{8} & \dfrac{9}{8} & -\dfrac{1}{24} \\ \dfrac{1}{4} & -\dfrac{1}{4} & -\dfrac{1}{4} & \dfrac{1}{4} \\ -\dfrac{1}{6} & \dfrac{1}{2} & -\dfrac{1}{2} & \dfrac{1}{6} \end{pmatrix} \begin{pmatrix} \xi_{-2-2} & \xi_{-2-1} & \xi_{-20} & \xi_{-21} \\ \xi_{-1-2} & \xi_{-1-1} & \xi_{-10} & \xi_{-11} \\ \xi_{0-2} & \xi_{0-1} & \xi_{00} & \xi_{01} \\ \xi_{1-2} & \xi_{1-1} & \xi_{10} & \xi_{11} \end{pmatrix}$$
$$\times \begin{pmatrix} -\dfrac{1}{16} & \dfrac{1}{24} & \dfrac{1}{4} & -\dfrac{1}{6} \\ \dfrac{9}{16} & -\dfrac{9}{8} & \dfrac{1}{4} & \dfrac{1}{2} \\ \dfrac{9}{16} & \dfrac{9}{8} & -\dfrac{1}{4} & -\dfrac{1}{2} \\ -\dfrac{1}{16} & -\dfrac{1}{24} & \dfrac{1}{4} & \dfrac{1}{6} \end{pmatrix} \tag{21}$$

$$\begin{pmatrix} \beta_{00} & \beta_{01} & \beta_{02} & \beta_{03} \\ \beta_{10} & \beta_{11} & \beta_{12} & \beta_{13} \\ \beta_{20} & \beta_{21} & \beta_{22} & \beta_{23} \\ \beta_{30} & \beta_{31} & \beta_{32} & \beta_{33} \end{pmatrix} = \begin{pmatrix} -\dfrac{1}{16} & \dfrac{9}{16} & \dfrac{9}{16} & -\dfrac{1}{16} \\ \dfrac{1}{24} & -\dfrac{9}{8} & \dfrac{9}{8} & -\dfrac{1}{24} \\ \dfrac{1}{4} & -\dfrac{1}{4} & -\dfrac{1}{4} & \dfrac{1}{4} \\ -\dfrac{1}{6} & \dfrac{1}{2} & -\dfrac{1}{2} & \dfrac{1}{6} \end{pmatrix} \begin{pmatrix} \eta_{-2-2} & \eta_{-2-1} & \eta_{-20} & \eta_{-21} \\ \eta_{-1-2} & \eta_{-1-1} & \eta_{-10} & \eta_{-11} \\ \eta_{0-2} & \eta_{0-1} & \eta_{00} & \eta_{01} \\ \eta_{1-2} & \eta_{1-1} & \eta_{10} & \eta_{11} \end{pmatrix}$$
$$\times \begin{pmatrix} -\dfrac{1}{16} & \dfrac{1}{24} & \dfrac{1}{4} & -\dfrac{1}{6} \\ \dfrac{9}{16} & -\dfrac{9}{8} & \dfrac{1}{4} & \dfrac{1}{2} \\ \dfrac{9}{16} & \dfrac{9}{8} & -\dfrac{1}{4} & -\dfrac{1}{2} \\ -\dfrac{1}{16} & -\dfrac{1}{24} & \dfrac{1}{4} & \dfrac{1}{6} \end{pmatrix} \tag{22}$$

For a square grid with unit length, equation (30) can be simplified as:

$$
\begin{aligned}
\Delta g_P &= \Delta g_\xi + \Delta g_\eta \\
&= \frac{1}{160\sqrt{2}\pi}(360\gamma\,(-2\alpha_{12} + 3\alpha_{30}) + 486\gamma\alpha_{32} \\
&\quad + \sqrt{2}(480\gamma \arcsin h[1]\alpha_{10} \\
&\quad + 720\gamma \arcsin h[1]\alpha_{12} + 27\gamma\,(18 \arcsin h[1]\alpha_{32} \\
&\quad - \arcsin h[1](20\alpha_{30} + 9\alpha_{32}))) \\
&\quad + 6\gamma(80\sqrt{2}\arcsin h[1]\beta_{01} + 90(2 \\
&\quad - \sqrt{2}\arcsin h[1])\beta_{03} \\
&\quad - 3(2 - 2\sqrt{2}\arcsin h[1])(20\beta_{21} + 27\beta_{23})).
\end{aligned}
\tag{32}
$$

III. NUMERICAL EXPERIMENT AND DISCUSSION

In this paper, a non-singular transformation is introduced to transform a singular integral into non-singular form so that we can invert a gravity anomaly from satellite altimetry data. This method has great practical significance as it may improve the accuracy of gravity anomaly inversion. In this section, we compare the numerical integration using (equation (38)) and without using (equation (37)) the non-singular transformation. The geoid height is given by the theoretical model and is used to evaluate the accuracy of the formula after the non-singular transformation.

A. TESTING WITH A THEORETICAL MODEL

To simplify the computation and intuit the analysis, we denote the singular integral in the inverse Vening Meinesz formula method as *IV*:

$$
IV = \iint_\sigma \frac{\xi_Q \cdot x + \eta_Q \cdot y}{(x^2 + y^2)^{3/2}} dxdy.
\tag{33}
$$

The geoidal height can be written as:

$$
N_Q = \sqrt{x^2 + y^2 + \delta^2}, (\delta > 0)
\tag{34}
$$

where δ is the initial geoidal height.

Fig. 5 shows the geoidal height for $\delta = 1, 5, 10$ and 100 m. When $\delta = 1$m, the geoidal height is in the range 1–1.732 m, spanning 0.732 m. When $\delta = 5$m, the geoidal height is in the range 5–5.196 m, with an interval of 0.196 m. When $\delta = 10$m, the geoidal height is in the range 10–10.0995 m, with an interval of 0.0995 m. Finally, when $\delta = 100$ m, the geoidal height is in the range 100–100.0099 m, with an interval of 0.0099 m. It can be seen that the geoidal height becomes smooth with an increase of δ.

The deflections of the vertical ξ_Q and η_Q can be expressed as:

$$
\xi_Q = -\frac{\partial N}{\partial x} = -\frac{x}{\sqrt{x^2 + y^2 + \delta^2}},
\tag{35}
$$

$$
\eta_Q = -\frac{\partial N}{\partial y} = -\frac{y}{\sqrt{x^2 + y^2 + \delta^2}}.
\tag{36}
$$

In this section, to simplify the computation, the innermost zone was modelled as a unit square domain where $\sigma \in [-1 < x < 1, -1 < y < 1]$. The integral *IV* without the non-singular transformation becomes

$$
\begin{aligned}
IV_1 &= \iint_\sigma \frac{\xi_Q \cdot x + \eta_Q \cdot y}{(x^2 + y^2)^{3/2}} dxdy \\
&= -\iint_\sigma \frac{1}{\sqrt{x^2 + y^2}\sqrt{x^2 + y^2 + \delta^2}} dxdy \\
&= -4\int_0^1 \int_0^1 \frac{1}{\sqrt{x^2 + y^2}\sqrt{x^2 + y^2 + \delta^2}} dxdy.
\end{aligned}
\tag{37}
$$

$$
\begin{aligned}
\Delta g_P &= \Delta g_\xi + \Delta g_\eta \\
&= \frac{1}{160m^2\sqrt{1+m^2}\pi}(m(180(m + m^3)\gamma(-2\alpha_{12} + 3m^2\alpha_{30}) + 243m(-2 + m^2 + 3m^4)\gamma\alpha_{32} \\
&\quad + \sqrt{1+m^2}(-480m^3\gamma\log[\frac{m}{1+\sqrt{1+m^2}}]\alpha_{10} + 360\gamma(\arcsin h[m] + m^3(-\log[m] + \log[1] + \sqrt{1+m^2}))\alpha_{12} \\
&\quad + 27\gamma(\arcsin h[m] + m^3(18\arcsin h[m]\alpha_{32} + m^5(\log[m] - \log[1 + \sqrt{1+m^2}])(20\alpha_{30} + 27\alpha_{32}))) \\
&\quad + 6\gamma(80m^2\sqrt{1+m^2}\arcsin h[m]\beta_{01} + 90(m + m^3 - \sqrt{1+m^2}\arcsin h[m])\beta_{03} \\
&\quad - 3m^2(m + m^3 + \sqrt{1+m^2}(-\arcsin h[m] + m^3(\log[m] - \log[1 + \sqrt{1+m^2}])))(20\beta_{21} + 27\beta_{23})))
\end{aligned}
\tag{30}
$$

$$
\begin{aligned}
\Delta g_{1\times1} &= \frac{1}{480m^2}(480m^3\log(\frac{1+\sqrt{1+m^2}}{m})\alpha_{1,0} - 40m\sqrt{1+m^2}\alpha_{1,2} + 60m^3\sqrt{1+m^2}\alpha_{3,0} - 6m\sqrt{1+m^2}\alpha_{3,2} \\
&\quad + 9m^3\sqrt{1+m^2}\alpha_{3,2} - 40m\sqrt{1+m^2}\beta_{1,2} - 40m^3(-12\log(\frac{1+\sqrt{1+m^2}}{m})\beta_{1,0} + \log(\frac{m}{1+\sqrt{1+m^2}})(\alpha_{1,2} + \beta_{1,2})) \\
&\quad + 60m^3\sqrt{1+m^2}\beta_{3,0} - 6m\sqrt{1+m^2}\beta_{3,2} + 9m^3\sqrt{1+m^2}\beta_{3,2} + 2\log(m + \sqrt{1+m^2})(20\alpha_{1,2} + 3\alpha_{1,2} + 20\beta_{1,2} + 3\beta_{3,2}) \\
&\quad + 3m^5\log(\frac{m}{1+\sqrt{1+m^2}})(20\alpha_{3,0} + 3\alpha_{3,2} + 20\beta_{3,0} + 3\beta_{3,2})).
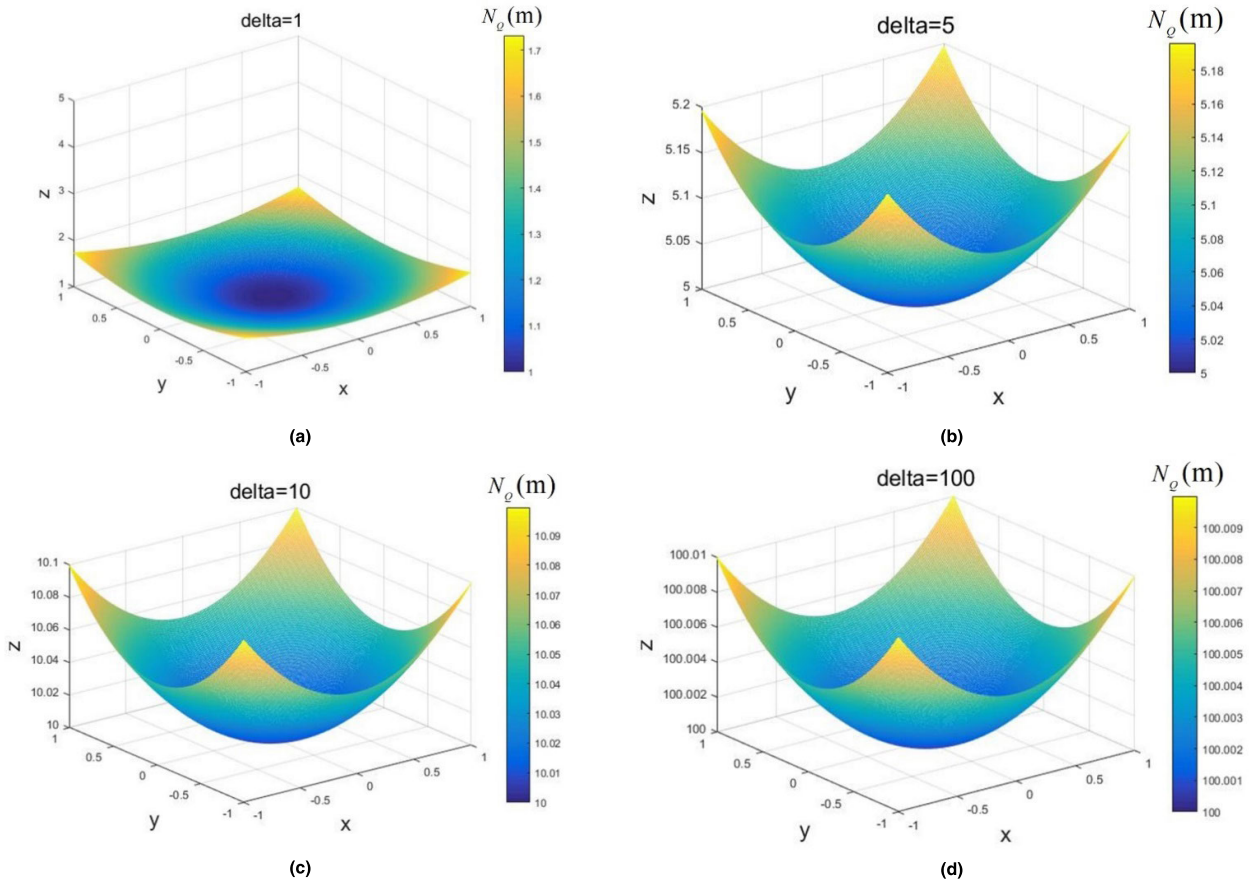\end{aligned}
\tag{31}
$$

FIGURE 5. Geoidal height with (a) $\delta = 1$ m, (b) $\delta = 5$ m, (c) $\delta = 10$ m, and (d) $\delta = 100$ m.

TABLE 1. Results of singular integrals IV_1 and IV_2 (in 10^{-6} m/s^2).

δ (m)	$N \times N$	4×4	10×10	200×200	600×600	800×800	1000×1000
1	IV_1	−3.7938	−4.8026	−5.9288	−6.0025	−6.0130	−6.0196
	IV_2	−5.4157	−5.8034	−6.0382	−6.0463	−6.0473	−6.0479
5	IV_1	−0.9630	−1.1559	−1.3743	−1.3888	−1.3909	−1.3922
	IV_2	−1.3312	−1.3723	−1.3970	−1.3978	−1.3979	−1.3982
10	IV_1	−0.4869	−0.5828	−0.6916	−0.6989	−0.6999	−0.7005
	IV_2	−0.6721	−0.6914	−0.7030	−0.7034	−0.7034	−0.7035
100	IV_1	−0.0489	−0.0584	−0.0693	−0.0700	−0.0701	−0.0702
	IV_2	−0.0674	−0.0693	−0.0704	−0.0705	−0.0705	−0.0705

Substituting equations (26) and (27) into equation (37), the integral using the non-singular transformation is IV_2. The results for the singular integral with and without using the non-singular transformation are shown in Table 1.

$$IV_2 = -4 \int_0^1 \int_0^1 \frac{1}{\sqrt{x^2 + y^2}\sqrt{x^2 + y^2 + \delta^2}} \mathrm{d}x\mathrm{d}y$$
$$= -4 \int_0^1 \int_0^1 \frac{1}{\sqrt{1 + k^2}\sqrt{x^2 + k^2 x^2 + \delta^2}} \mathrm{d}x\mathrm{d}k$$

$$-4 \int_0^1 \int_0^1 \frac{1}{\sqrt{1 + \lambda^2}\sqrt{\lambda^2 y^2 + y^2 + \delta^2}} \mathrm{d}\lambda\mathrm{d}y$$
$$= -8 \int_0^1 \int_0^1 \frac{1}{\sqrt{1 + k^2}\sqrt{x^2 + k^2 x^2 + \delta^2}} \mathrm{d}x\mathrm{d}k. \quad (38)$$

As illustrated in Table 1, the accuracy of IV_2 for 10×10 is roughly the same as the accuracy of IV_1 for 200×200. Therefore, the efficiency of equation (38), which
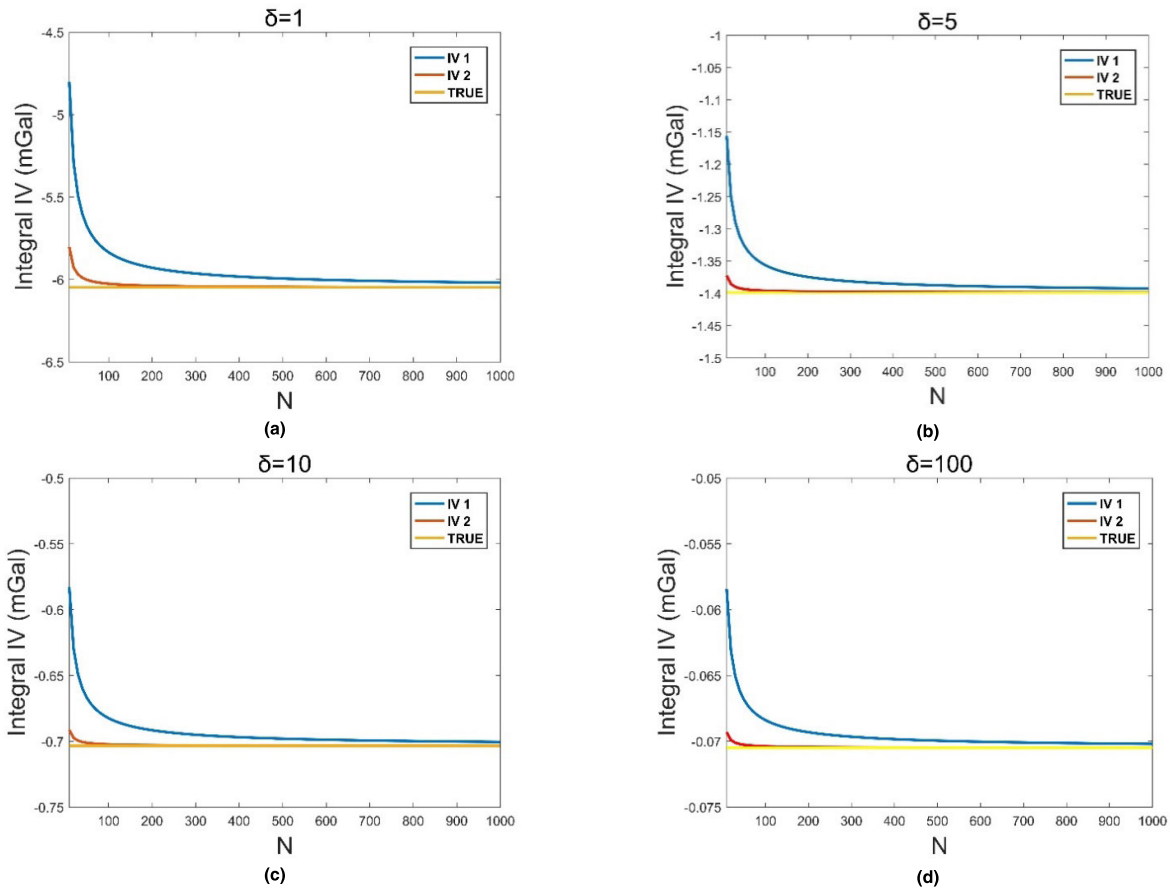
FIGURE 6. Results for the singular integral with and without the non-singular transformation for (a) $\delta = 1$ m, (b) $\delta = 5$ m, (c) $\delta = 10$ m, and (d) $\delta = 100$ m.

TABLE 2. Comparisons between the results of the singular integral *IV* using the non-singular transformation and exact values.

δ (m)	Exact value (10^{-6} m/s^2)	*IV* (10^{-6} m/s^2)	Absolute error (10^{-6} m/s^2)	Relative error
1	−6.0479	−5.9717	0.0762	1.26%
5	−1.3982	−1.3896	0.0086	0.62%
10	−0.7035	−0.7064	0.0029	0.41%
100	−0.0705	−0.0705	0.0000	0.00%

uses a non-singular transformation, is improved compared with (37), which does not use the transformation.

Fig. 6 shows the results of numerical integration with and without the non-singular transformation for $\delta = 1, 5, 10$, and 100 m, for different partitions from 4×4 to 1000×1000. As illustrated in Fig. 6, the efficiency of equation (37) without the non-singular transformation is lower than the efficiency of equation (38) with the transformation. Moreover, the convergence speed is slow in the lower partitions from 4×4 to 400×400. The convergence speed of equation (38) using the transformation is fast and the result is close to the true value. From Fig. 6 and Table 1, it can be seen that equation (38) using the non-singular transformation is more efficient, converges faster, and is more accurate for evaluating the gravity anomaly. Therefore, the non-singular transformation is useful for the singular integration of the Earth's gravity field.

According to equation (31), when the deflections of the vertical are expressed using bicubic interpolation, the computation for singular integral is

$$
\begin{aligned}
IV = \frac{1}{80}[&480 \ln(1 + \sqrt{2})(\alpha_{10} + \beta_{01}) \\
&- 360(\sqrt{2} - 2\ln(1 + \sqrt{2}))(\alpha_{12} + \beta_{21}) \\
&+ 540(\sqrt{2} - \ln(1 + \sqrt{2}))(\alpha_{30} + \beta_{03}) \\
&+ 243(\sqrt{2} - \ln(1 + \sqrt{2}))\alpha_{32} \\
&- 486(\sqrt{2} - 2\ln(1 + \sqrt{2}))\beta_{23}],
\end{aligned}
\tag{39}
$$

where $\alpha_{10}, \alpha_{12}, \alpha_{30}, \alpha_{32}, \beta_{01}, \beta_{21}, \beta_{03}$, and β_{23} are given by equations (21) and (22).

The error for *IV* is compared in Table 2 with the result for IV_2 at 1000×1000, which is considered to be the exact value.

Table 2 shows the absolute and relative errors between the singular integral using the non-singular transformation and
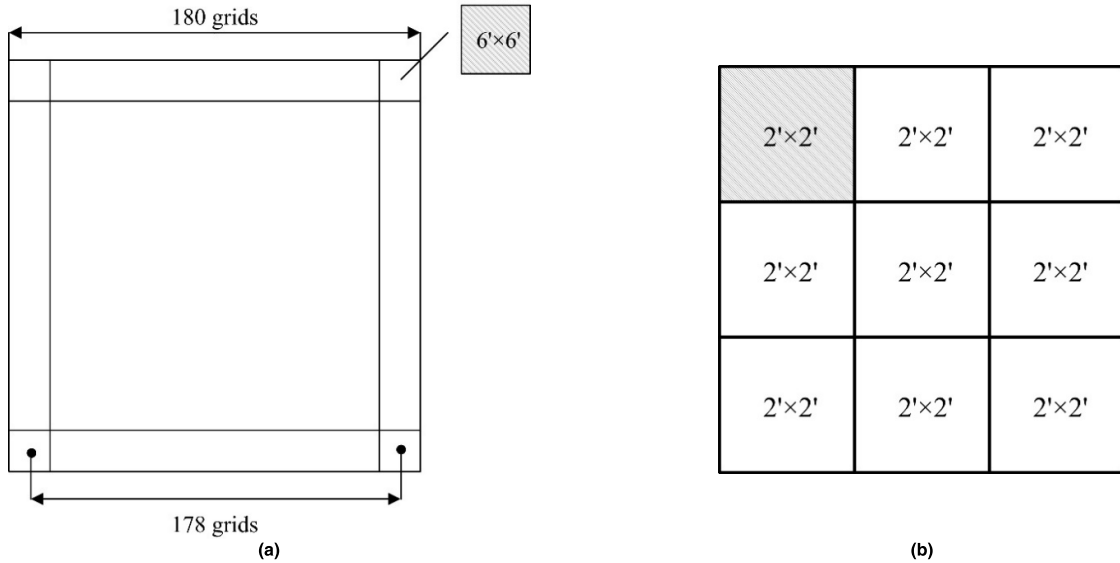
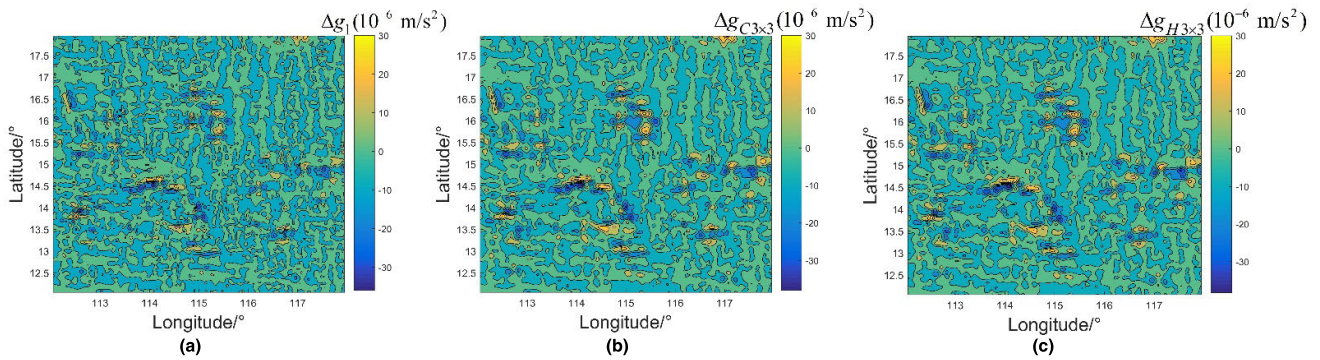FIGURE 7. (a) Computational zone for the vertical data. (b) The innermost zone of the vertical data.

FIGURE 8. Gravity anomaly in the innermost zone for a grid of 6' × 6' by (a) this paper Δg_1, (b) Hwang's method $\Delta g_{H3\times3}$, (c) Chang's method $\Delta g_{C3\times3}$.

the exact values. The absolute and relative errors are 0.0762×10^{-6} m/s^2 and 1.26% for $\delta = 1$ m, 0.0086×10^{-6} m/s^2 and 0.62% for $\delta = 5$m, 0.0029×10^{-6} m/s^2 and 0.41% for $\delta = 10$m, and 0 for $\delta = 100$m. The errors decrease with an increase of δ, which indicates that they depend on the undulations of the geoid. The absolute and relative errors are smaller in a smoother area. In general, the relative error of the numerical integration with the non-singular transformation is less than 1.5%, which is significantly higher than that without the non-singular transformation. Thus, the results of the numerical integration using the non-singular transformation are satisfactory for a practical application.

B. TESTING WITH ACTUAL DATA

To further investigate the effects of the innermost zone on the inversion of a gravity anomaly, this paper used satellite altimeter data. The test area for this application of the inverse Vening Meinesz formula was the South China Sea and its vicinity (12°N–18°N, 112°E–118°E). The practical computation is based on deflections of the vertical with

a resolution of 2' × 2' in the low latitude area. The computational and innermost zones of the vertical data are illustrated in Fig. 7.

There are 180 × 180 grid elements in the test area. In this work, we consider the innermost zone as a grid of 6' × 6' (giving a grid of 3 × 3), as shown in Fig. 7(b). We applied equations (11) of Hwang's [24], (12) of Chang *et al.* [9] and (30) to evaluate the contribution of the innermost zone to the gravity anomaly in the 178 × 178 grid [Fig. 7(a)]. The results are $\Delta g_{H3\times3}$, $\Delta g_{C3\times3}$ and Δg_1, respectively. Moreover, we consider the innermost zone as a grid of 2' × 2' (giving a grid of 1 × 1) and apply equations (11), (12) and (31) to evaluate the contribution of the innermost zone to the gravity anomaly in the 178 × 178 grid. The results are $\Delta g_{H1\times1}$, $\Delta g_{C1\times1}$ and Δg_2, respectively. The gravity anomalies $\Delta g_{C3\times3}$, $\Delta g_{H3\times3}$, Δg_1, $\Delta g_{C1\times1}$, $\Delta g_{H1\times1}$ and Δg_2 in the innermost zone are shown in Figs. 8 and 9, respectively.

Fig. 8 indicates that with a grid of 6' × 6', the range for the gravity anomalies in the innermost zone in the South China
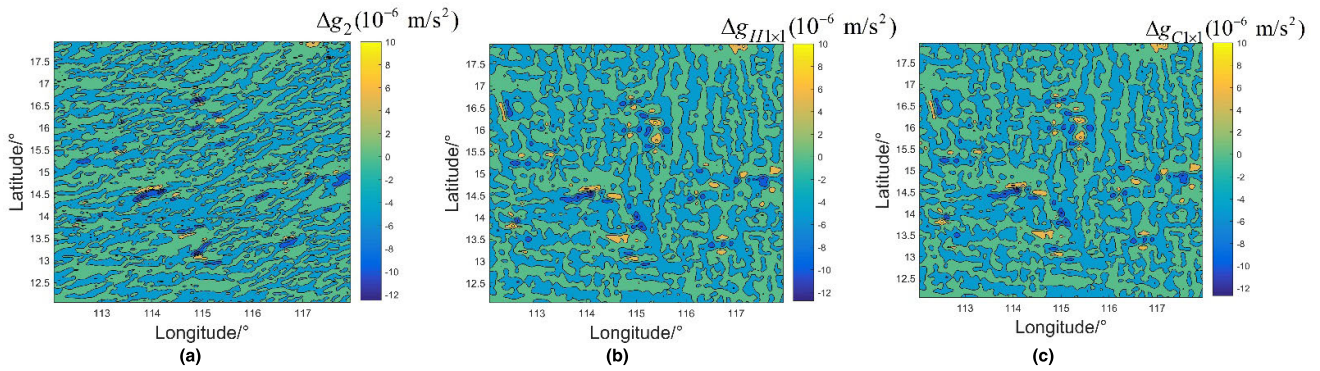
FIGURE 9. Gravity anomaly in the innermost zone for a grid of 2' × 2' by(a)this paper Δg_2, (b) Hwang's method $\Delta g_{H1\times1}$, (c)Chang's method $\Delta g_{C1\times1}$.

TABLE 3. Statistics of the gravity anomalies in the innermost zone (in 10^{-6} m/s^2).

Gravity anomaly	Max	Min	Mean	SD
Δg_1	32.563	−36.023	0.086	4.928
$\Delta g_{H3\times3}$	35.761	−38.228	0.129	5.945
$\Delta g_{C3\times3}$	35.761	−38.018	0.128	5.912
Δg_2	13.660	−12.501	0.015	1.744
$\Delta g_{H1\times1}$	13.920	−12.743	0.043	1.982
$\Delta g_{C1\times1}$	13.855	−12.673	0.043	1.971

Sea can reach more than $\pm30 \times 10^{-6}$ m/s^2, which has effect to the gravity anomalies in the test zone. Moreover, the trends of gravity anomalies in the three figures are consistent. The gravity anomalies are clearly visible. Compared with the results of Fig. 8(b) and 8(c), the changes of gravity anomalies in Fig. 8(a) are more detailed. It illustrates that the method which expressed the deflections of the vertical in the form of double cubic polynomials is more accurately to calculated the gravity anomalies at the dynamic integration points in the innermost zone, that is because this method used 16 points around the dynamic integration point for interpolation calculation, rather than the average of 4 points around the dynamic integration point.

In Fig. 9, for a grid of 2' × 2', the range for the gravity anomalies can reach more than $\pm10 \times 10^{-6}$ m/s^2. The gravity map in Fig. 9 changes relatively smoothly compared to Fig. 8, but the trend of gravity anomalies is consistent. Thus, the size of the gravity anomalies in the innermost zone depends on the grid dimensions in that zone. According to the experimental result, even if the integral range is given as a grid of 1 × 1, the maximum and minimum gravity anomaly of the dynamic integral point in the innermost zone can reach more than $\pm10 \times 10^{-6}$ m/s^2, therefore, the effect of the innermost zone on the gravity anomalies cannot be ignored.

The standard deviation (SD), maximum (max), minimum (min), and mean of $\Delta g_{C3\times3}$, $\Delta g_{H3\times3}$, Δg_1, $\Delta g_{C1\times1}$, $\Delta g_{H1\times1}$ and Δg_2 are shown in Table 3. The SD, maximum,

minimum, and mean of Δg_1 are 4.928 × 10^{-6} m/s^2, 32.563 × 10^{-6} m/s^2, −36.023 × 10^{-6} m/s^2, and 0.086 × 10^{-6} m/s^2, respectively. The SD, maximum, minimum, and mean of $\Delta g_{H3\times3}$ are 5.945 × 10^{-6} m/s^2, 35.761 × 10^{-6} m/s^2, −38.228 × 10^{-6} m/s^2, and 0.129 × 10^{-6} m/s^2, respectively. The SD, maximum, minimum, and mean of $\Delta g_{C3\times3}$ are 5.912 × 10^{-6} m/s^2, 35.761 × 10^{-6} m/s^2, −38.018 × 10^{-6} m/s^2, and 0.128 × 10^{-6} m/s^2, respectively. The SD, maximum, minimum, and mean of Δg_2 are 1.744 × 10^{-6} m/s^2, 13.660 × 10^{-6} m/s^2, −12.501 × 10^{-6} m/s^2, and 0.015 × 10^{-6} m/s^2, respectively. The SD, maximum, minimum, and mean of $\Delta g_{H1\times1}$ are 1.982 × 10^{-6} m/s^2, 13.92 × 10^{-6} m/s^2, −12.743 × 10^{-6} m/s^2, and 0.043 × 10^{-6} m/s^2, respectively. The SD, maximum, minimum, and mean of $\Delta g_{C1\times1}$ are 1.971 × 10^{-6} m/s^2, 13.855 × 10^{-6} m/s^2, −12.673 × 10^{-6} m/s^2, and 0.043 × 10^{-6} m/s^2, respectively. The SD of $\Delta g_{H3\times3}$ and $\Delta g_{H1\times1}$ by using Hwang's method [24] and $\Delta g_{C3\times3}$ and $\Delta g_{C1\times1}$ by using Chang's method [9] are not as small as that of this paper, whether the integral range is given a grid of 1 × 1 or 3 × 3. Moreover, the absolute values of the maximum and minimum are Hwang's method Chang's method are larger than those of this paper. Therefore, the discreteness of the computed results in this paper of the gravity anomalies in the innermost zone are small. This is related to the selection of interpolation points in interpolation calculation. A certain number of interpolation points and the uniform distribution of interpolation points can make the calculation result more accurate.

Compared the range for the gravity anomalies for a grid of 6' × 6' with a grid of 2' × 2'. The SD of Δg_2 is not as large as that of Δg_1. The maximum of Δg_2 is less than that of Δg_1. Even so, the absolute values of the maximum and minimum are still more than 10 × 10^{-6} m/s^2. These results indicate that the grid in the innermost zone makes an important contribution to the inversion of gravity anomalies. Thus, setting the integral kernel function to zero in the innermost zone, as done by the traditional algorithms, affects the accuracy of gravity inversion, and the innermost zone must be considered. Equation (31) can be used to compute the contribution of the 1 × 1 grid in which the computational

point is a gravity anomaly, which can improve the accuracy of gravity inversion. Moreover, it should be noted that the region around the dynamic integral point has practical significance for its calculation.

IV. CONCLUSION

We improved the accuracy of the inversion of gravity anomalies in the innermost zone using the inverse Vening Meinesz formula. We introduced the non-singular transformation and expressed the deflections of the vertical using bicubic interpolation by treating the innermost zone as a rectangle. A precise formula for the innermost zone of the rectangular domain, which is more consistent with the actual data distribution, was then derived. The efficiency, convergence, and accuracy of this algorithm and the influence of the central area were assessed with a theoretical model and with actual data.

1.Using the non-singular transformation, the singular integral in the inverse Vening Meinesz formula can be transformed into a non-singular integral, which can be integrated numerically. The problem is solved that the dynamic integral points in the innermost zone cannot be integrated. The results show that the accuracy of the formula using the non-singular transformation is better than 1.5%, and is significantly higher than without the non-singular transformation. The non-singular transformation may also be useful for other situations with singular integrals relating to the Earth's gravity field.

2. Deflections of the vertical are expressed using a bicubic interpolation. The innermost zone is treated as a rectangle. Formulas for computing the gravity anomalies of this area were derived using the non-singular transformation. The numerical tests with the theoretical model show that the formula has high accuracy and can achieve satisfactory results in a practical application.

3. A practical computation based on deflections of the vertical for data with a resolution of 2' × 2' from the South China Sea and its vicinity show that the integral kernel function is not zero in the innermost zone. The discreteness of the computed results in this paper of the gravity anomalies in the innermost zone are small. The non-singular transformation has a non-negligible contribution in the computation of a gravity anomaly in the innermost zone. The region around the dynamic integral point has practical significance for its calculation.

REFERENCES

[1] C. Zhu, J. Guo, J. Gao, X. Liu, C. Hwang, S. Yu, J. Yuan, B. Ji, and B. Guan, "Marine gravity determined from multi-satellite GM/ERM altimeter data over the south China sea: SCSGA V1.0," *J. Geodesy*, vol. 94, no. 5, p. 50, May 2020.

[2] *OSTM/Jason-2 Products Handbook*, NASA, CNES, JPL, Washington, DC, USA, 2009.

[3] J. Dorandeu, M. Ablain, Y. Faugère, F. Mertz, B. Soussi, and P. Vincent, "Jason-1 global statistical evaluation and performance assessment: Calibration and cross-calibration results," *Mar. Geodesy*, vol. 27, nos. 3–4, pp. 345–372, Jul. 2004.

[4] M. Ablain, S. Philipps, N. Picot, and E. Bronner, "Jason-2 global statistical assessment and cross-calibration with Jason-1," *Mar. Geodesy*, vol. 33, no. 1, pp. 162–185, 2010.

[5] Y. Faugere, J. Dorandeu, F. Lefevre, N. Picot, and P. Femenias, "ENVISAT ocean altimetry performance assessment and cross-calibration," *Sensors*, vol. 6, no. 3, pp. 100–130, Mar. 2006.

[6] P. Prandi, S. Philipps, V. Pignot, and N. Picot, "SARAL/AltiKa global statistical assessment and cross-calibration with Jason-2," *Mar. Geodesy*, vol. 38, no. 1, pp. 297–312, 2015.

[7] X. Wan, R. F. Annan, S. Jin, and X. Gong, "Vertical deflections and gravity disturbances derived from HY-2A data," *Remote Sens.*, vol. 12, no. 14, p. 2287, Jul. 2020.

[8] W. Cui, W. Wang, Z. Jie, J. Yang, and Y. Jia, "Improvement of sea surface height measurements of HY-2A satellite altimeter using Jason-2," *Mar. Geodesy*, vol. 41, no. 6, pp. 632–648, Nov. 2018.

[9] X.-T. Chang, J.-C. Li, C.-Y. Zhang, Y.-M. Dang, and J.-G. Hu, "Deduction and estimation of innermost zone effects in altimetry gravity algorithm," *Chin. J. Geophys.*, vol. 48, no. 6, pp. 1302–1307, 2005.

[10] J. Li, J. Ning, and J. Chen, "Determination of gravity anomalies over the South China Sea by combination of TOPEX/Poseidon, ERS2 and GeoSat altimeter data," *Acta Geodaetica et Cartographica Sinica*, vol. 30, no. 3, pp. 197–202, 2001.

[11] M.-T. Huang, G.-J. Zhai, Y.-Z. Ouyang, X.-P. Lu, C.-Y. Liu, and T.-Q. Wu, "Recovery of marine gravity field using integrated data from multi-satellite mission," *Sci. Surv. Mapping*, vol. 31, no. 6, pp. 37–39, 2006.

[12] M. T. Huang, G. Zhai, and Z. Guan, "On the recovery of gravity anomalies from altimeter data," *Acta Geodaetica et Cartographica Sinica*, vol. 30, no. 2, pp. 179–184, 2001.

[13] H. T. Hsu, H. Y. Wang, and G. Y. Wang, "Geoid undulations and gravity anomalies from T/P and ERS-1 altimeter data in the China Sea and vicinity," *Chin. J. Geophys.*, vol. 1999, no. 4, pp. 3–5, 1999.

[14] D. T. Sandwell, R. D. Müller, W. H. F. Smith, E. Garcia, and R. Francis, "New global marine gravity model from CryoSat-2 and Jason-1 reveals buried tectonic structure," *Science*, vol. 346, no. 6205, pp. 65–67, Oct. 2014.

[15] D. Sandwell, E. Garcia, K. Soofi, P. Wessel, M. Chandler, and W. H. F. Smith, "Toward 1-mGal accuracy in global marine gravity from CryoSat-2, ENVISAT, and Jason-1," *Lead. Edge*, vol. 32, no. 8, pp. 892–899, 2013.

[16] O. B. Andersen, "KMS2002 global marine gravity field, bathymetry and mean sea surface," in *Proc. AGU Fall Meeting Abstr.*, 2003, pp. 56–58.

[17] O. B. Andersen, P. Knudsen, and P. A. M. Berry, "The DNSC08GRA global marine gravity field from double retracked satellite altimetry," *J. Geodesy*, vol. 84, no. 3, pp. 191–199, Mar. 2010.

[18] C. Hwang, E.-C. Kao, and B. Parsons, "Global derivation of marine gravity anomalies from SeaSat, GeoSat, ERS-1 and TOPEX/POSEIDON altimeter data," *Geophys. J. Int.*, vol. 134, no. 2, pp. 449–459, 2015.

[19] G. S. Gopalapillai, "Non-global recovery of gravity anomalies from a combination of terrestrial and satellite altimetry data," Ph.D. dissertation, Dept. Geodetic Sci., Ohio State Univ., Columbus, OH, USA, 1974.

[20] D. T. Sandwell and W. H. F. Smith, "Marine gravity anomaly from GeoSat and ERS 1 satellite altimetry," *J. Geophys. Res.*, vol. 102, no. B5, pp. 10039–10054, 1997.

[21] R. Rummel, "The determination of gravity anomalies from geoid height using the inverse Stokes's formula," Ph.D. dissertation, Dept. Geodetic Sci., Ohio State Univ., Columbus, OH, USA, 1977.

[22] O. B. Anderson and P. Knudsen, "Global marine gravity field from the ERS-1 and GeoSat geodetic mission altimetry," *J. Geophys. Res.*, vol. 103, no. C4, pp. 8129–8137, 1988.

[23] S. F. Bian, "Numerical solution for geodetic boundary value problem and the Earth's gravity field approximation," Ph.D. dissertation, Inst. Surveying Mapping, Wuhan Tech. Univ. Surv. Mapping, Wuhan, China, 1992.

[24] C. Hwang, "Inverse Vening Meinesz formula and deflection-geoid formula: Applications to the predictions of gravity and geoid over the South China Sea," *J. Geodesy*, vol. 72, pp. 304–314, May 1988.

[25] C. Hwang, H.-Y. Hsu, and R.-J. Jang, "Global mean sea surface and marine gravity anomaly from multi-satellite altimetry: Applications of deflection-geoid and inverse Vening Meinesz formulae," *J. Geodesy*, vol. 76, no. 8, pp. 407–418, Nov. 2002.

[26] E. A. Boyarsky, L. V. Afanasieva, and V. N. Koneshov, "Method to compute the vertical deflection component," in *Gravity, Geoid and Earth Observation* (International Association of Geodesy Symposia), vol. 135, S. Mertikas, Eds. Berlin, Germany: Springer, 2010, doi: 10.1007/978-3-642-10634-7_55.

[27] H. Sunkel, "Die darstellung geodtischer integral formeln durch bi-kubische spline funktionen," Folge 28, Int. Assoc. Geodesy, Graz, Austria, Tech. Rep., 1977.

[28] Y. Wang, "Problem der glattung bei den integraloperation der physikallischen geodasie," Folge 55, Naturwissenschaften, Graz, Austria, Tech. Rep., 1987.

[29] S. Bian and H. Sun, "The expression of common singular integrals geodesy," *Manuscripta Geodaetica*, vol. 19, no. 2, pp. 62–69, 1994.

[30] W. A. Heiskanen and H. Moritz, *Physical Geodesy*. San Francisco, CA, USA: Springer, 1967.

[31] S. Bian, "Some cubature formulas for singular integrals in physical geodesy," *J. Geodesy*, vol. 71, pp. 443–445, Jul. 1997.

[32] J. L. Awange and E. W. Grafarend, *Solving Algebraic Computational Problems in Geodesy and Geoinformatics*. Stuttgart, Germany: Springer, 2005.

[33] S. Bian and H. Li, "Mathematical analysis of some typical problems in geodesy by means of computer algebra," in *Trends in Geomatics*, R. Abdalla, Ed. London, U.K.: IntechOpen, 2019, pp. 67–87.

ZONG JINGWEN (Member, IEEE) received the Ph.D. degree from the Naval University of Engineering. His main research interests include satellite altimetry and gravity-aided navigation. His expertise lies in satellite altimetry and gravity matching navigation research.

BIAN SHAOFENG received the Ph.D. degree from Wuhan University, in 1995. He is currently a Professor of geodesy and navigation with the Naval University of Engineering, China. His current research interests include physical geodesy, precise positioning using GNSS, gravity-aided navigation, and transformation of map projections. Later that year, he was awarded an Alexander Von Humboldt Research Fellowship.

LI HOUPU received the Ph.D. degree in satellite navigation from the Naval University of Engineering, China, in 2010. He is currently an Associate Professor of navigation with the Naval University of Engineering. His research interests include satellite altimetry, geodesy, and map projection.

JI BING received the Ph.D. degree in satellite navigation from the Naval University of Engineering, China, in 2011. He is currently an Associate Professor of navigation with the Naval University of Engineering. His research interests include using gravity gradients for underwater navigation and exploration.

OUYANG YONGZHONG is currently a Professor with the Key Laboratory of Marine Environmental Survey Technology and Application. His research interest includes gradient detection theory for marine gravity and its application. His expertise lies in gravity, inversion theory, and underwater terrain detection.

• • •